View metadata, citation and similar papers at core.ac.uk

brought to you by CORE

provided by University of Lincoln Institutional Repository

Photochemical & Photobiological Sciences

An international journal

www.rsc.org/pps

Volume 9 | Number 2 | February 2010 | Pages 117–264

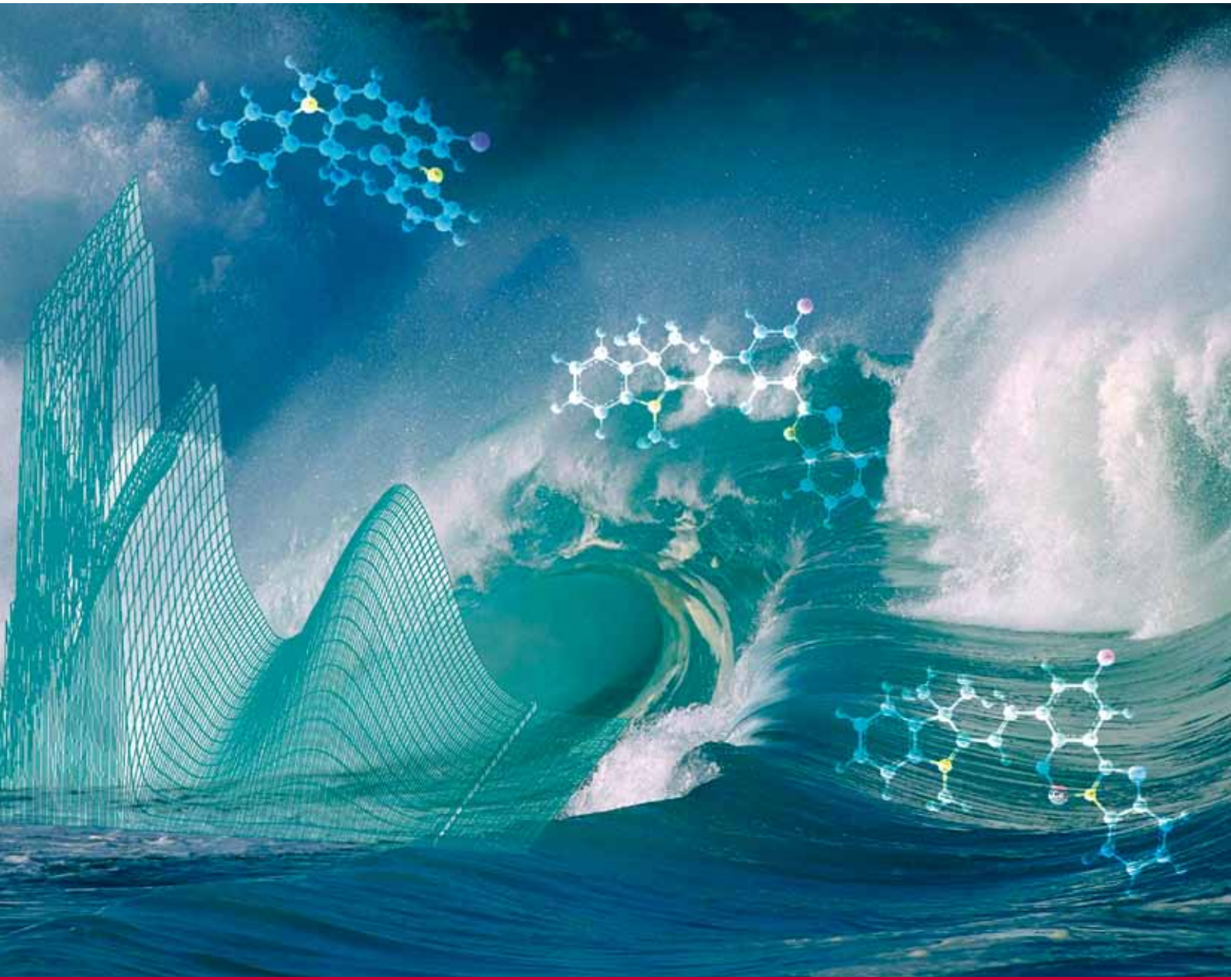

Themed Issue: Synthetic and natural photoswitches

ISSN 1474-905X

RSC Publishing

1474-905X(2010)9:2;1-Z

Transient Brewster angle reflectometry of spiropyran monolayers†

Sergey Gorelik,*[a] Song Hongyan,[a,b] Martin J. Lear[b] and Jonathan Hobley*[a]

Received 18th September 2009, Accepted 13th November 2009
First published as an Advance Article on the web 15th December 2009
DOI: 10.1039/b9pp00105k

Brewster angle reflectometry has been developed as a tool for determining the absorbance and refractive index changes in molecular monolayers containing spiropyran. The method is sensitive to changes in both the real and imaginary parts of the refractive index in the monolayers. It was used to monitor the conversion of spiropyran to merocyanine and the reversal of this reaction when the molecules were immobilised on quartz using silane coupling. An analytical solution of Fresnel formula allowed the transient reflectometry data to be converted into transient absorption information. Absorbances of transients as low as ~10^{-6} were possible using the current apparatus with a single laser pulse transient measurement. It was found that spiropyran photoconverted to merocyanine with an efficiency of ~0.1. The photochemical reversion of converted merocyanine to spiropyran occurred with efficiencies of 0.03–0.2 and this was probably site dependent. It was found that the thermal conversion from merocyanine to spiropyran was slow and even after 10 min there was no significant thermal reversion. This measurement was possible because the real part of the refractive index of the monolayer could be monitored with time using an off-resonance probe at a wavelength where the merocyanine did not absorb light meaning that the probe did not photobleach the sample. Thus our method also provides a non-intrusive method for probing changes in molecules in thin films.

A. Introduction

Spiropyran (SP) conversion to merocyanine (MC) (Scheme 1) in monolayers on solid supports and in Langmuir and Langmuir Blodgett films has been extensively studied because of its potential for use in photoswitching applications.[1–10] For example the switchability has been harnessed to make the wetability of surfaces change, in order to alter capillary action, to lift heads of liquid, and to make water droplets move as UV and visible light excitation are alternated.[1–3] Light-induced phase transitions and pressure jumps have also been observed on timescales from minutes to hours,[4–6] as well as more recently by the current authors using nanosecond time-resolved Brewster angle microscopy.[7–9] Furthermore SP's ability to switch surface properties has been utilized in electrodes on gold for binding proteins,[10] in biopolymer films[11] and in hybrid surface architectures.[12]

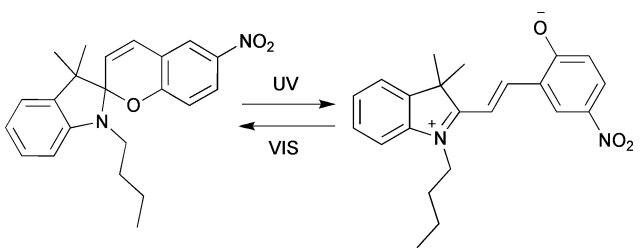

Scheme 1 Schematic representation of SP to MC and reverse photoconversions.

[a]*Institute of Materials Research and Engineering, A*STAR (Agency for Science, Technology and Research), 3 Research Link, Singapore 117602*
[b]*Department of Chemistry, and Medicinal Chemistry Program of the Life Sciences Institute, National University of Singapore, 3 Science Drive 3, Singapore 117543*

† This paper is part of a themed issue on synthetic and natural photoswitches.

Despite the plethora of works harnessing or studying the photo-switching of properties by SP, as well as other molecules,[13] on surfaces, there is little fundamental knowledge about the photochemical reactions themselves. This is primarily because making optical measurements in thin films and monolayers is difficult due to the short optical pathlength available. Ellipsometry has been reported on SP thin-films.[14,15] Reflectometry based on surface plasmon resonance (SPR) has been used to monitor reactions in self-assembled monolayers[16] and in polymer films[17] on metallic gold and silver surfaces, however the vast majority of surfaces are not metallic, so it is desirable to find alternative means to probe reactions in monolayers that can be used on a wider range of substrates.

Diffuse reflectance has been successfully applied to studying monolayers on scattering media[18] and this methodology was developed in the late 1980s into picosecond and nanosecond diffuse reflectance flash photolysis by Wilkinson *et al.*[19,20] The measurement relies on multiple scattering in an opaque medium, meaning that the effective pathlength is increased. This method is especially useful since many surfaces scatter light diffusely. Later still, regular reflectance flash photolysis was proposed by Fukumura *et al.* to look at specular reflection from highly absorbing thick molecular samples.[21]

More recent attempts to look at absorbance in ultra-thin films have applied the methods of waveguides to observe ~100-fold increases in sensitivity using multiple passes.[22] Also, cavity ring-down has been applied to this problem using multiple passes through the film and the substrate to gain extra pathlength.[23–28] This has resulted in measurements of absorbance down to 10^{-6} per laser pulse (better with averaging) with the drawbacks that the time resolution of the technique will be limited and the problem that small absorbances in the substrate can interfere in the measurement. The method has therefore not been applied for kinetic studies. Katoh *et al.*[29,30] have also developed methodologies

in transient absorption using electronic filtering that have pushed down absorbance change detection limits in transmission to ~10^{-6} with multiple accumulations of transient signals.

Note that, although highly sensitive, both cavity ring-down and Katoh's methods monitor transmitted light. This is most appropriate for bulk measurements and thicker films, although cavity ring-down methods have also been applied to monolayers. However all molecular monolayers are deposited on bulk substrates; and even very low level traces of absorbing or scattering impurities in the substrate will contribute at the same level as the monolayer or even higher. Reflection, on the other hand, is naturally more sensitive to optical properties of interfaces than the transmission. One of the most accurate and widely used techniques to measure optical properties of thin films at bulk interfaces is ellipsometry. However, when using this method for monolayers it is not always possible to separate optical constants such as absorption coefficient, refractive index and the monolayer's thickness.[31]

Another useful technique for measuring low absorbances in thin films is polarization modulation reflection spectroscopy,[32] which can measure absorbances down to 10^{-6} using lock-in amplification and signal modulation. This will, however mean that the data must be accumulated over some time. According to ref. 32, for a monolayer on gold, peak to peak noise of 5×10^{-5} can be obtained with 200 background scans and 1000 sample scans using this technique.

Brewster angle microscopy (BAM), itself a special case of ellipsometry, was invented by Henon *et al.* and Hönig *et al.* to observe monolayers.[33,34] So, not surprisingly, it is well suited for the study of optical transformations in these thin films.[7–9] The method relies on the fact that when p-polarized light is incident on an interface of two transparent media at the Brewster angle it is nearly all refracted and reflectivity is at a minimum. If the refractive index of the interface changes the minimum reflectivity angle or value will change. Hence it is possible to observe and image very small changes in refractive index.

In the current work we describe the use of reflectometry in the vicinity of the Brewster angle to make transient measurements in thin films. Using this method, with a single transient generating nanosecond laser pulse shot, absorbance sensitivities of ~10^{-6} have been achieved demonstrating that this it is at least a competitive and complimentary technique to cavity ring down or any other proposed methods. Furthermore, it has some potential advantages, such as being inherently more versatile to kinetic studies and less susceptible to scattering losses from the bulk of the substrate. The measurement is more approaching dark-field as the measurement is made in geometries for which the intrinsic levels of reflected light are low. The data is easily interpretable as a kinetic trace of reflectance, which has proportionality to concentration, with time. Furthermore the reflectance is sensitive to both real and imaginary parts of refractive index and this method will yield independent assessment of both of these parameters. An additional advantage is that the BAM technique can also be used in pump–probe imaging mode with μm space resolution.[7–9]

In the current work, the BAM method combined with pulsed laser excitation has been used to elucidate relevant photochemical parameters of the photocolouration, photobleaching and thermal fading reactions for the system of SP immobilised onto fused silica using silane coupling reagents. Thus this method opens an alternative way in which to study the photochemistry of monolayers in which the absorbance changes are otherwise extremely difficult to measure. Absorbance sensitivities down to ~10^{-6} are demonstrated for single laser pulse transient measurements.

B. Experimental

1. Chemical synthesis

In this section the synthesis of the spiropyran, 5-(3′,3′-dimethyl-6-nitrospiro[chromene-2,2′-indoline]-1′-yl)pentanoic acid ($C_{23}H_{23}N_2O_7$), is described (Scheme 2), as well as the immobilization procedure by covalently bonding it to the surface of fused silica (FS) slides (Scheme 3).

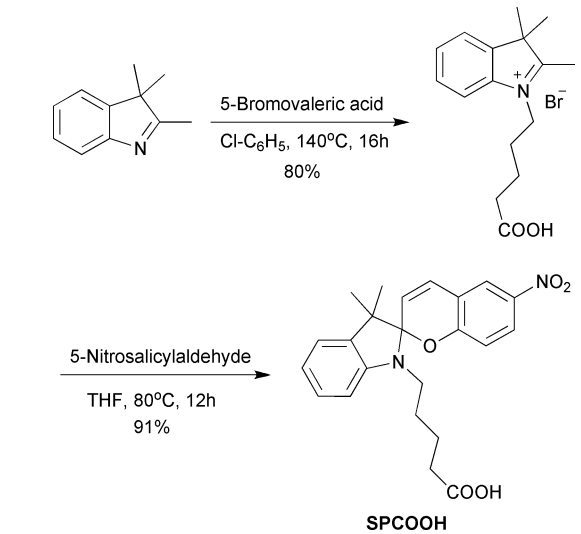

Scheme 2 Synthesis of SPCOOH.

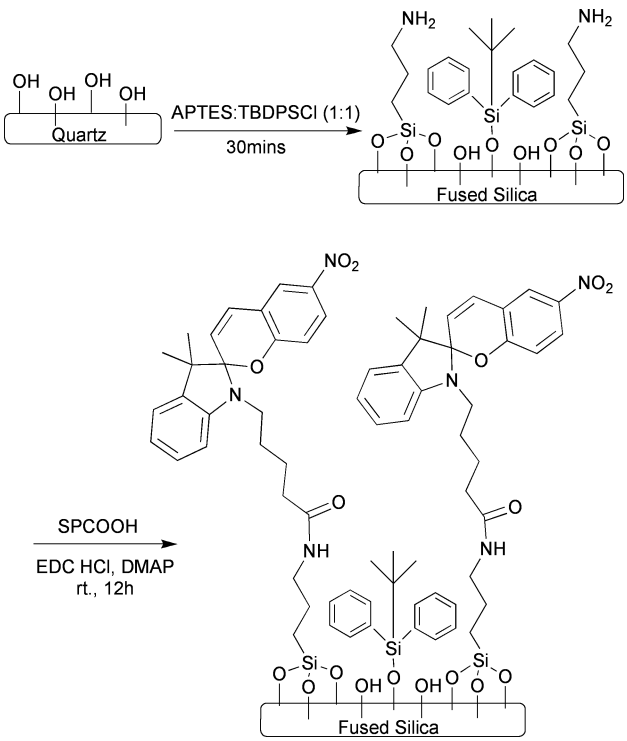

Scheme 3 Procedure of FS slide modification with SPCOOH.

 This journal is © The Royal Society of Chemistry and Owner Societies 2010

1-(4-Carboxybutyl)-2,3,3-trimethyl-3*H*-indolium bromide. A solution of 2,3,3-trimethylindolenine (1.71 g, 10.8 mmol) and 5-bromovaleric acid (2.14 g, 11.8 mmol) in 5 ml of chlorobenzene was heated at 140 °C for 16 h. After cooling to room temperature, the mixture was titrated with 100 mL of acetone. After a few minutes, a light pink solid came out. The solid was filtered out and washed with acetone to give 2.87 g (8.64 mmol, 80% yield) of the desired indolium bromide as a light pink solid: ^{1}H NMR (500 MHz, DMSO-d_6) δ 1.54 (6H, s, 2-CH_3), 1.65 (2H, m, $CH_2CH_2CH_2CH_2COOH$), 1.86 (2H, m, $CH_2CH_2CH_2CH_2COOH$), 2.31 (2H, t, J = 7 Hz, $CH_2CH_2CH_2CH_2COOH$), 2.85 (3H, s, –CH_3), 4.49 (2H, t, J = 8 Hz, $CH_2CH_2CH_2CH_2COOH$), 7.6–8.0 (4H, m, ArH); ^{13}C NMR (125 MHz, DMSO-d_6) δ 14.3, 21.8, 22.4, 27.0, 33.4, 47.6, 54.5, 115.8, 123.9, 129.3, 129.8, 141.5, 142.2, 174.4, 197.0; IR (neat, cm^{-1}): 2875, 1732, 1597, 1401, 1298; HRMS (ESI) m/z [M – Br]$^+$: calcd 260.1645, obsd 260.1643 for $C_{16}H_{22}O_2N_1$.

5-(3′,3′-Dimethyl-6-nitrospiro[chromene-2,2′-indoline]-1′-yl)pentanoic acid (SPCOOH). A solution of 1-(4-carboxybutyl)-2,3,3-trimethyl-3*H*-indolium bromide (118 mg, 0.347 mmol) and 5-nitrosalicylaldehyde (64 mg, 0.382 mmol) in 10 mL of THF was heated at 80 °C for 12 h. After cooling to room temperature, a dark purple solid precipitated. The solid was filtered and the filter cake was washed with ether to give 129 mg (0.316 mmol, 91% yield) of SPCOOH as dark red solid: ^{1}H NMR (300 MHz, $CDCl_3$) δ 1.18 (3H, s, 3-CH_3), 1.28 (3H, s, 3-CH_3), 1.64 (4H, m, $CH_2CH_2CH_2CH_2COOH$), 2.34 (2H, t, J = 7 Hz, $CH_2CH_2CH_2CH_2COOH$), 3.19 (2H, m, $CH_2CH_2CH_2CH_2COOH$), 5.86 (1H, d, J = 10 Hz, Pyran-H), 6.56 (1H, d, J = 8 Hz, ArH), 6.74 (1H, d, J = 8 Hz, ArH), 6.86 (1H, d, J = 7 Hz, ArH), 6.90 (1H, d, J = 10 Hz, Pyran-H), 7.07–7.21 (2H, m, ArH), 8.00–8.03 (2H, m, ArH); ^{13}C NMR ^{13}C NMR (75 MHz, $CDCl_3$) δ 19.8, 22.4, 26.0, 28.3, 33.5, 43.3, 52.6, 106.6, 115.5, 118.4, 119.5, 121.7, 121.9, 122.7, 125.9, 127.7, 128.2, 135.9, 140.9, 147.0, 159.5, 178.4; IR (neat, cm^{-1}): 1699, 1609, 1512, 1479, 1274; HRMS (ESI) m/z [M+H]$^+$: calcd 409.1758, obsd 409.1762 for $C_{23}H_{25}O_5N_2$; m/z [M + Na]$^+$ calcd 431.1577, obsd 431.1582 for $C_{23}H_{24}O_5N_2{}^{23}Na_1$.

FS slide modification with SPCOOH. The FS slides were cleaned by pyrolysis in a furnace at 500 °C for 5 h to remove any organic contamination prior to use. 3-Aminopropyltriethoxysilane (APTES) was used as a silane coupling agent and *tert*-butyldiphenylsilyl (TBDPS) was used as a spacer. The APTES and *tert*-butylchlorodiphenylsilane (TBDPSCl) were mixed in different proportion to alter the SP surface coverage as required. Solutions of APTES/TBDPSCl in dry toluene (0.25% v/v) were prepared. The slides were then incubated in the solution at room temperature for 30 min to obtain the aminated slides. After amination, the silane-coated slides were incubated in an ethanolic solution of SPCOOH in the presence of EDC (10 molar equivalents). This was carried out in an airtight bottle, at room temperature, with gentle shaking for 12 h. The slides were then removed from the solution and washed sequentially with ethanol and water to remove unbound SPCOOH.

2. The apparatus for reflectometry

The apparatus (Fig. 1) is a modified NanoFilm EP^3 BAM. A CW probe laser (532 nm or 671 nm AOTK diode lasers ~50 mW appropriately attenuated using filters) is made incident at the air interface with the sample monolayer in the vicinity of the interface's Brewster angle.

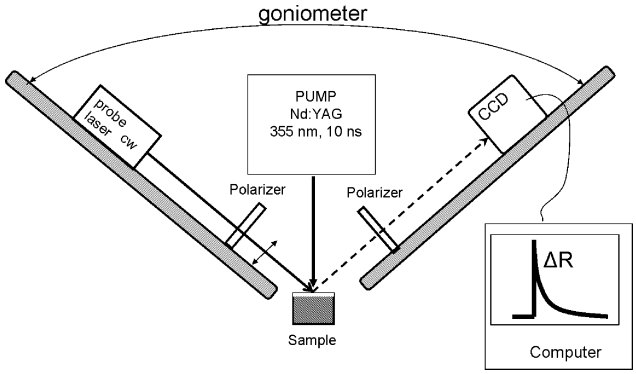

Fig. 1 Experimental setup for time-resolved Brewster angle reflectometry.

The probe light is p-polarization purified before the sample using a high extinction (1×10^{-8}) Glan-Thompson polarizer. In the current work, the reflected beam is collected with the microscope's objective removed and monitored using a CCD camera. The CCD camera can measure images every 40 ms, enabling real-time monitoring of events occurring on timescales from 40 ms up to a few seconds.

This timescale is adequate in the current study. However, for faster timescales either faster cameras, photomultiplier tubes, or pump–probe imaging can be used.[7–9] The angle of incidence is varied using the EP^3 goniometer, which has a 0.01° angle resolution and a reproducibility of 0.001°.

The 355 nm, 5 ns pulse from a Lotis Nd-YAG laser is made incident normal to the surface and the sample monolayer. This initiates photo-induced reactions in the monolayer. The laser pulse energy fluence could be varied from 0–100 mJ cm^{-2}.

A Shimadzu UV-2450 UV-VIS spectrometer was used to measure the absorption spectrum of the initial SP monolayer.

3. Theoretical considerations for data handling

Numerically, the reflectivity of the interface can be simulated using Fresnel equations,[7] however, in the following we have derived its analytical approximation that simplifies the approach for quantification of kinetic studies. For this derivation, we consider a monolayer to be a thin homogeneous isotropic film with a refractive index n_1 and thickness d at the interface of two transparent media with refractive indices n_0 for the upper medium and n_2 for the lower medium.

The probe light is p-polarized and incident from the upper medium (medium 0) to the film (medium 1) at an angle θ_0 (Fig. 2). In the film it is refracted at an angle θ_1 and in the lower medium (medium 2) it is refracted at θ_2. The angles are related according to the Snelius law: $n_i \sin\theta_i = n_k \sin\theta_k$.[35a] Then the Fresnel equation for reflectance of p-polarized light from a thin film at an interface between two infinite media can be used:[35b]

$$R(\theta_0) = \left| \frac{r_{01} + r_{12} e^{-2i\beta}}{1 + r_{01} r_{12} e^{-2i\beta}} \right|^2 \quad (1)$$

where

$$r_{01} = \frac{n_1 \cos\theta_0 - n_0 \cos\theta_1}{n_1 \cos\theta_0 + n_0 \cos\theta_1} \quad (2)$$

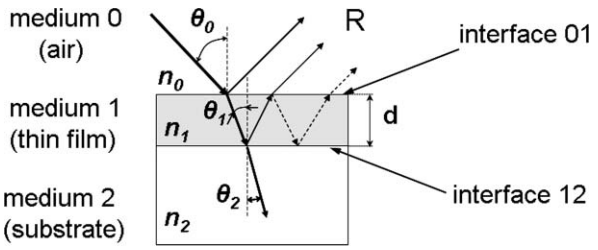

Fig. 2 The schematic representation of the monolayer film.

is the reflectivity from the pure interface 01 between media 0 and 1 and

$$r_{12} = \frac{n_2 \cos\theta_1 - n_1 \cos\theta_2}{n_1 \cos\theta_2 + n_2 \cos\theta_1} \tag{3}$$

is the reflectivity from the pure interface 12 between media 1 and 2.

$$\beta = \frac{2\pi}{\lambda} d n_1 \cos\theta_1 \tag{4}$$

is the phase factor, λ is the wavelength of the incident light.

Instead of plotting the monolayer's reflectance as a function of the angle of incidence, in further considerations it will be convenient to plot it against the reflectivity of the pure interface 02, which is itself a function of the angle of incidence

$$r_{02} = \frac{n_2 \cos\theta_0 - n_0 \cos\theta_2}{n_2 \cos\theta_0 + n_0 \cos\theta_2} \tag{5}$$

We assume that the film is initially transparent, that is the initial refractive index n_{10} is real. Upon pulsed UV irradiation, transient species are formed and the refractive index becomes complex, if the transients absorb the probe light:

$$n_1 = n_{10} + \Delta n(t) - ik(t), \tag{6}$$

where the imaginary part is an extinction coefficient, k, which is proportional to the absorption coefficient α.[35c]

$$k = \alpha\lambda/4\pi \tag{7}$$

Thus the two parameters that change upon photo-excitation are the real and the imaginary parts of the refractive index of the film. They will both contribute to the change of the reflectance:

$$\Delta R(\theta_0,t) = R(\theta_0,t) - R_0(\theta_0) \tag{8}$$

where $R_0(\theta_0)$ is the initial reflectance before the irradiation.

To estimate these contributions, we assume that, in the vicinity of Brewster angle, the parameters d/λ, $\Delta n/n_{10}$, k/n_{10}, r_{02} are small ($\ll$1). That d/λ is small is obvious because we are dealing with a monolayer and this assumption will be safe up to a few tens of nanometres. r_{02} is related to the angle of incidence which we can control, so we can keep it small. Likewise $\Delta n/n_{10}$, k/n_{10} can be limited by limiting the excitation fluence. For example, in the current work this holds true for photoconversions up to 50% (*vide infra*). Then we can carry out the Taylor series expansion of the Fresnel equation (1) over these parameters. As noted above, the result of the Taylor series expansion for the first non-vanishing terms can be most simply expressed using r_{02} as an independent variable instead of the angle of incidence θ_0:

$$\Delta R(r_{02}) = Ar_{02} + B \tag{9}$$

$$A = 4\pi \frac{d}{\lambda} n_{10} \frac{\left(1 - \frac{n_0^2 n_2^2}{n_{10}^4}\right)}{\sqrt{n_0^2 + n_2^2}} k \tag{10}$$

$$B = \left(2\pi \frac{d}{\lambda} n_{10}\right)^2 n_{10} \frac{\left(1 - \frac{n_0^2 n_2^2}{n_{10}^4}\right)\left(1 - \frac{n_0^2}{n_{10}^2}\right)\left(1 - \frac{n_2^2}{n_{10}^2}\right)}{n_0^2 + n_2^2} \Delta n \tag{11}$$

Eqn (9)–(11) therefore predict that ΔR is linear with respect to r_{02} and that the slope is proportional to k, whilst the intercept is proportional to Δn. Thus, using this approximation, it is possible to separate the contributions of Δn and k to ΔR. This prediction will be experimentally validated later in the results and discussion section (*vide infra*).

Combining eqn (7) and (10), the coefficient A can be expressed in terms of the monolayer's absorbance Abs = αd:

$$A = n_{10} \frac{\left(1 - \frac{n_0^2 n_2^2}{n_{10}^4}\right)}{\sqrt{n_0^2 + n_2^2}} \mathrm{Abs} \tag{12}$$

where Abs corresponds to the absorbance at the normal incidence of the probe light to the monolayer, but not the real absorbance at the real angle of incidence. Taking into account that the monolayer is one molecule thick, Abs = σN, where σ is the absorption cross-section of the transient (cm^2) and N is its surface concentration (cm^{-2}).

Note, that k and Δn are derived keeping only the first non-vanishing terms in the Taylor series approximation of the exact Fresnel equation (1). Comparison of k and Δn values calculated using eqn (9)–(11) with numerically simulated reflectance using the exact Fresnel equation (1) showed that the error in the approximation is about 10%. For better precision the next terms in the Taylor series expansion have to be derived.

4. Data collection procedure

The procedure required for data collection is dictated by the need to experimentally obtain the time dependent parameters A and B for eqn (9)–(12) as well as parameters for the initial monolayer (its initial refractive index n_{10} and its thickness d). The rigorous data collection procedure involves three steps.

a. Reflectance calibration. In the first step of the procedure, the angle dependence of reflectance of a pure interface $R'_{02}(\theta_0)$ is measured, in greyscale units of the CCD, in the vicinity of the Brewster angle. First, the variable substitution is required $\theta_0 \leftarrow r_{02}$. This is easy to achieve using eqn (5) since the values of n_0, n_2 are known. Then, the greyscale units must be converted into absolute reflectance units (R_{02}). R'_{02} is proportional to R_{02} *via* a calibration factor S:

$$R'_{02}(r_{02}) = SR_{02}(r_{02}) + \mathrm{DC} = S(r_{02}^2 + C) + \mathrm{DC} \tag{13}$$

 This journal is © The Royal Society of Chemistry and Owner Societies 2010

where DC is a dark current of the CCD camera. R_{02} is an exact parabola with regard to r_{02}, and C is an offset background, which includes a background reflection from the sample due to scattering, probe-beam divergence, *etc.* By fitting the dependence $R'_{02}(r_{02})$ with a parabolic function one can obtain S and C.

b. Evaluation of the initial monolayer parameters. In the second step, the r_{02} dependence of reflectance of the interface with the SP monolayer $R_{init}(r_{02})$ is measured by changing the angle of incidence in the vicinity of the Brewster angle. From this procedure using Fresnel equations (1)–(5), we can estimate the parameters of the initial monolayer, such as n_{10} and d.

c. Transient laser induced reflectometry measurements. In the third step, we irradiate the sample monolayer with the pump pulse at different angles of incidence in the vicinity of the Brewster angle, and record the kinetics of the reflectance change $\Delta R(t)$ at each specific angle. Thus we achieve $\Delta R(t,r_{02})$ and in principle we can record the evolution of the dependence $\Delta R(r_{02})$ with time. Finally, using formulae (9)–(11) to fit $\Delta R(r_{02})$ at each point in time, we can evaluate $k(t)$ and $\Delta n(t)$.

From $k(t)$ we can determine the kinetics of the system since k is proportional to the concentration of transients. Interpretation of the value of Δn is, however, not that straightforward and may be seen as a complicating factor that makes reflectance changes harder to analyse kinetically. However, in some cases the procedure for obtaining the kinetics can be simplified and Δn can be ignored as will be described to be the case for this SP/MC system using a 532 nm probe light.

When the first term in eqn (9), Ar_{02}, is much larger than the second one, B, we can neglect the second term and ΔR will become proportional to k and hence to the transient concentration. The first term in eqn (9) is proportional to r_{02}. Therefore, moving the angle of incidence away from the Brewster angle, and hence increasing $|r_{02}|$, we can often achieve the situation desired for simplified kinetic analysis. In that case, the reflectance change can be measured at a fixed angle of incidence, for which the first term of eqn (9) is dominant. If this is done the kinetics of the reflectance change will be a good guide to the kinetics of the transient concentrations of the system. Other parameters such as the excitation and probe fluence can be varied at this fixed angle.

C. Results and discussion

Fig. 3 shows the UV-VIS spectrum of an SP modified slide before (dotted line) and after (solid line) ~100 pulses of 355 nm irradiation (10 Hz, 10 mJ cm^{-2}). The dotted vertical lines show the wavelengths of the pump radiation, 355 nm and the probe radiation, 532 nm. Before irradiation the spectrum corresponds to that of SP with no MC; 355 nm is close to the absorption maximum. After irradiation a peak at 550 nm appears, which corresponds to MC absorption. From these spectra one can see that 532 nm is very close to the MC absorption maximum in the visible region.

Fig. 4 shows the UV-VIS spectrum of a typical sample slide used for the reflectometry measurements. Initially, all of the monolayer consists of SP only. The absorbance at ~355 nm is ~1.5×10^{-3}. This absorption spectrum was measured in transmission using a standard UV-Vis spectrometer. This means that the probe light passed through two chemically modified sides of the fused silica slide, so we can say that the absorbance of a single side of the slide

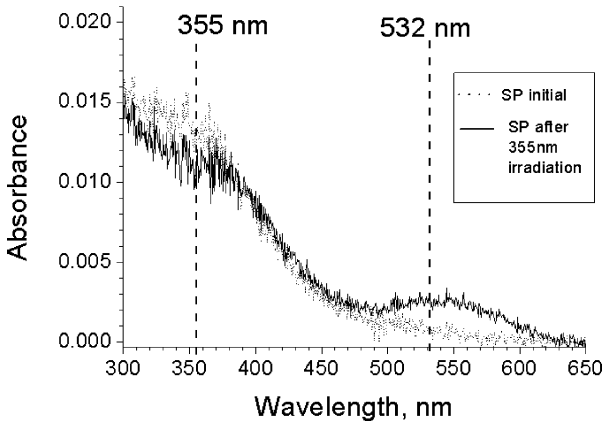

Fig. 3 UV-VIS spectrum of a SP modified slide before and after series of pulses of 355 nm irradiation. Dashed line: before the irradiation; solid line: after the irradiation.

is ~7.5×10^{-4}. Note that only one side is probed in the reflection measurement. This low absorbance makes the sample challenging to study using conventional means. Using a typical molar decadic absorption coefficient for SP in solutions ($\varepsilon \approx 4000$ L mol^{-1} cm^{-1}),[36] the SP surface concentration N_{sp} can be estimated: $N_{sp} \approx 1$ nm^{-2}.

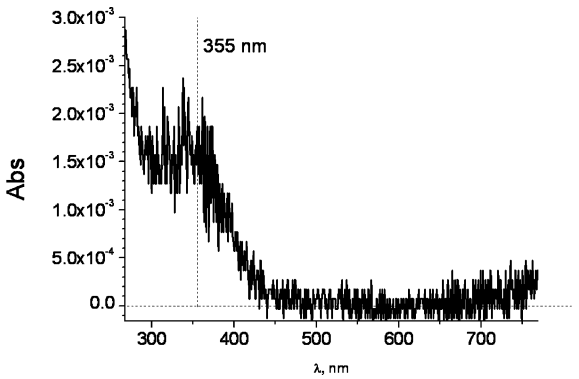

Fig. 4 UV-VIS spectrum of a typical SP modified slide used for the time-resolved reflectometry measurements.

Next, as the first step of the experimental procedure, the analysis of the r_{02} dependence of reflectance of the initial monolayer will be discussed. Refractive indices for air and FS are known to be $n_0 = 1$, $n_2 = 1.46$,[37] respectively, therefore it is easy to calculate the dependence $r_{02}(\theta_0)$. This is shown in Fig. 5 for θ_0 in the vicinity of the Brewster angle. The Brewster angle for an air/FS interface is $\theta_B = \arctan(n_2/n_0) = 55.6°$. $r_{02}(\theta_0)$ in the vicinity of θ_B is a straight line with a negative slope, and $r_{02}(\theta_B) = 0$. An example of the r_{02} dependence of a pure air/fused silica interface is shown in Fig. 6 with a dashed line (532 nm probe beam with intensity 2 mW cm^{-2}). The y-axis on the right corresponds to greyscale units of the CCD camera; the y-axis on the left corresponds to the absolute reflectance. The calibration factor $S = 1.3 \times 10^8$ was obtained by fitting the dependence with parabola (13). The background, C, was found to be ~10^{-7} under the experimental conditions used. The minimum of the parabola is found to be at $r_{02} = 0$, which corresponds to the Brewster angle.

Next, in the second step of the experimental procedure, we obtain an estimate for n_{10} and d for the initial condition as it is required in formulae (9)–(11) to enable us to determine the

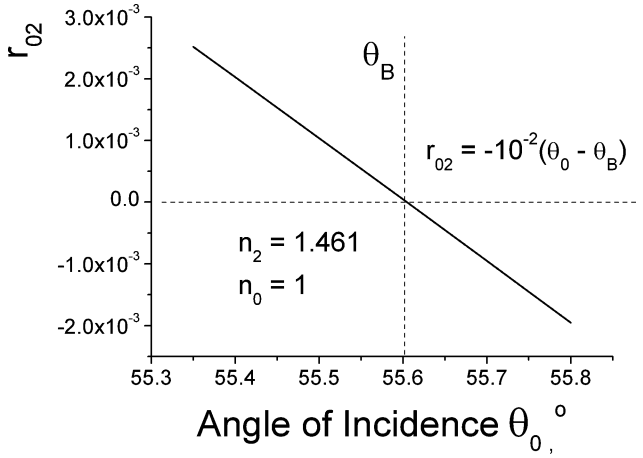

Fig. 5 Angle of incidence dependence of r_{02} in the vicinity of the Brewster angle for an air/FS interface.

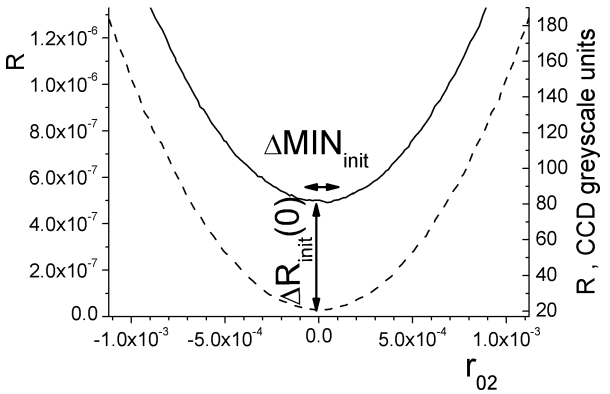

Fig. 6 The r_{02} dependences of the initial SP monolayer reflectance (solid line) and of the pure air/FS interface (dashed line). ΔMIN_{init} corresponds to the shift of the minimum of the former with respect to the minimum of the latter along the r_{02} axis. $\Delta R_{init}(0)$ corresponds to the shift of the minimums along the R axis. The right y-axis is in CCD greyscale units, and the left y-axis is in the actual reflectance units. The calibration procedure is described in the text.

absolute value of transient absorption and the real part of the refractive index change (k and Δn).

These values could be obtained independently, using other experimental methods, or from assumptions based upon the molecular structure. However, in principle, it is also possible to estimate their values with the current apparatus using the method described below, if other sources of the data are not available.

The reflectance dependence $R_{init}(r_{02})$ is shown in Fig. 6 by a solid line. The difference between $R_{init}(r_{02})$ and R_{02} is clear and much larger than the noise level.

$R_{init}(r_{02})$ has a pronounced minimum in the vicinity of $r_{02} = 0$. In general, it is possible to show, using Fresnel equations, that $R_{init}(r_{02})$ is a parabola, similar to R_{02}, however it is shifted 'vertically', by $\Delta R_{init}(0)$ and 'horizontally', by ΔMIN_{init} in the figure, with respect to $R_{02}(r_{02})$. The difference in the curvatures of the parabolas is quite negligible if $d \ll \lambda$, which is the case for a monolayer. Using these two parameters ($\Delta R_{init}(0)$, ΔMIN_{init}) it is possible to calculate n_{10} and d independently. For example, in the case when n_{10} is close to n_2, $(n_{10} - n_2)/n_2 \ll 1$, we can use the Taylor series expansion for the Fresnel equation using r_{02}, d/λ, $\Delta n = n_{10} - n_2$ as small parameters. The result for the first non-vanishing terms is similar to (9):

$$\Delta R_{init}(r_{02}) = A r_{02} + B \tag{14}$$

In this case the coefficients A and B will be:

$$A = 8\pi^2 \frac{\left(\frac{d}{\lambda}\right)^2 n_2}{2(n_0^2 + n_2^2)}\left(1 - \frac{n_0^2}{n_2^2}\right) \times \delta n \times r_{02} \tag{15}$$

$$B = 4\pi^2 \frac{\left(\frac{d}{\pi}\right)^2}{(n_0^2 + n_2^2)}\left(1 - \frac{n_0^2}{n_2^2}\right)^2 \times \delta n^2 \tag{16}$$

Hence, we can obtain δn from

$$\frac{B}{A} = \frac{1}{2n_2}\left(1 - \frac{n_0^2}{n_2^2}\right) \times \delta n \tag{17}$$

Thus d can be obtained either from (15) or (16). Fig. 7 shows the difference $\Delta R_{init}(r_{02})$ between $R_{init}(r_{02})$ and $R_{02}(r_{02})$ (shown in Fig. 6). Using the parameters of the linear fit to $\Delta R_{init}(r_{02})$ (solid line in Fig. 7) it was found that $d = 1.7$ nm and $\delta n = 0.08$, and hence that $n_{10} \approx 1.55$.

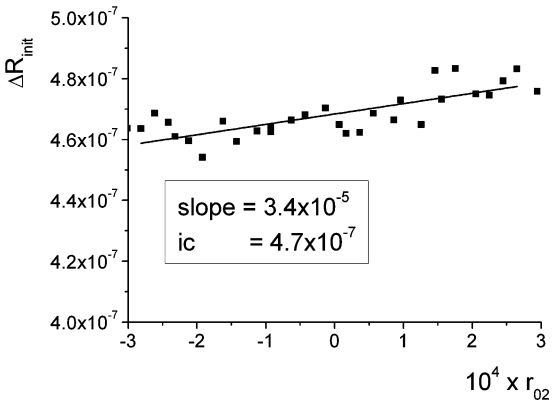

Fig. 7 The r_{02} dependence of the difference of the initial SP monolayer reflectance and the reflectance of the pure air/FS interface from Fig. 6. Dots: experimental data; solid line: linear fit to the data.

Note that, for such a thin film, ΔMIN_{init} is quite difficult to measure with high precision, since it is close to the limit of experimental reproducibility. For a film a few nanometres thick, it corresponds to a shift of the minimum of the angle of incidence dependence of a few millidegrees. Therefore, the values of δn and d obtained are a rough estimate. However, the values obtained appear to be quite reasonable values for this organic monolayer and will be used in further estimations.

Next, we will estimate the expected absorbance changes in the monolayer, after photoconversion, to evaluate weather our approximations (eqn (9)–(11)) are valid. To do this assume that the molar decadic absorption coefficient $\varepsilon \approx 40\,000$ L mol^{-1} cm^{-1} at 532 nm for MC, which is reasonable since values for the related 6,8-dinitro-substituted analogue, for which ε is best known, range from 35 000–45 000 L mol^{-1} cm^{-1} depending on the solvent.[38] The value that we currently adopt, 40 000 L mol^{-1} cm^{-1}, is from a measurement made in acetone. The surface of the fused silica is

 This journal is © The Royal Society of Chemistry and Owner Societies 2010

modified with alkyl, ketyl, amino and phenyl groups so it is hard to assign a polarity in this case. This is because there are polar, non-polar and polarizable groups all present. We therefore choose a medium value for ε. The absorbance of MC on the surface is close to maximum at ~532 nm (Fig. 3) so we can assume that the best value of ε is to use is that for the peak maximum as we have done. $n_{10} \approx 1.55$ and the estimated surface coverage of SP molecules is ~1 nm^{-2}. We can therefore expect that, even if 50% of all of the SP molecules in the monolayer convert to MC under the action of the pump radiation, the transient absorbance of MC formed will only be about 3×10^{-3} and $k/n_{10} \sim 0.04$ which is $\ll 1$. Therefore, the approximations (9)–(11) of Fresnel equation (1) can be used.

Next we discuss step 3 of the experimental procedure. Representative $\Delta R(t)$ dependences following single pulse 355 nm photoexcitation are shown in Fig. 8 at two different angles of incidence: 55.50° and 55.70°. The former one is smaller than the Brewster angle and corresponds to $r_{02} = 10^{-3}$, which is >0, and with $\Delta R(t)>0$, whilst the latter is larger than the Brewster angle and corresponds to $r_{02} = -10^{-3} < 0$, and with $\Delta R(t)<0$.

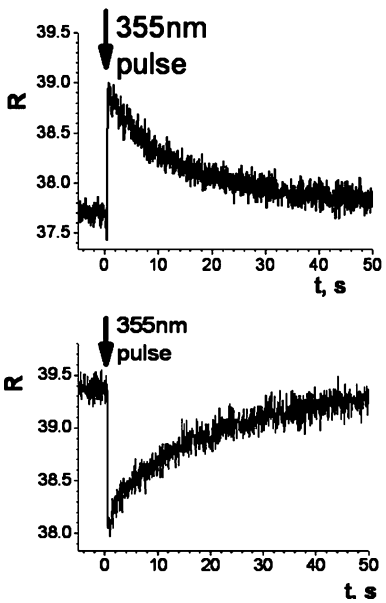

Fig. 8 Representative $\Delta R(t)$ dependences following a single 355 nm photoexcitation pulse (10 mJ cm^{-2}) at two different angles of incidence: (top) 55.50°; (bottom) 55.70°. The Brewster angle is about 55.60°. Probe light wavelength is 532 nm, intensity 2 mW cm^{-2}.

Both kinetic traces have similar characteristic decay times. At $r_{02} = 0$, $\Delta R(t)$ is not detectable above the noise level. Both dependences were obtained using 532 nm probe light with a fluence of 2 mW cm^{-2}.

The representative $\Delta R(t)$ dependence for the 671 nm probe light taken at $r_{02} = 0$ is shown in Fig. 9. At other values of r_{02}, $\Delta R(t)$ was found to be similar. Note that a 671 nm probe fluence of about 500 mW cm^{-2} was required in order to see a ΔR signal with similar in magnitude to that seen in case of the 532 nm probe of 2 mW cm^{-2}. Note also that there is some drift in the long term stability of the diode laser currently employed leading to kinks in the kinetic trace over such long timescales.

In the case of the 671 nm probe light, even though the fluence was so high, ΔR did not change with time within the time interval

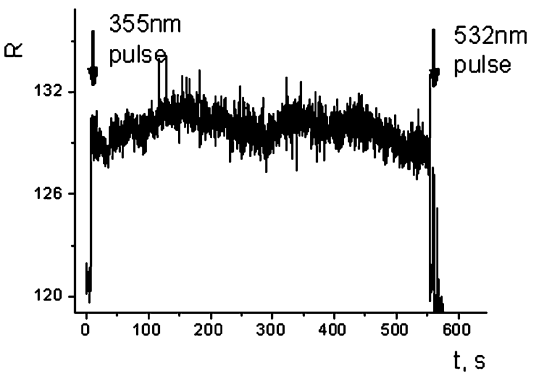

Fig. 9 Representative $\Delta R(t)$ dependences following a single 355 nm photoexcitation pulse (10 mJ cm^{-2}) with the 671 nm probe taken at the Brewster angle, 55.60°. Probe light intensity is about 500 mW cm^{-2}. A 532 nm laser switched the monolayer back at ~550 s.

of measurement of about 10 min. So, no reverse thermal reaction occurred on this time scale. The fast drop in ΔR in the end of the trace corresponds to the moment when a 532 nm laser was made incident normal to the sample at the same time as the 671 nm probe. This laser switched the monolayer back to the original non-coloured state. This means that, the main reason for the ΔR decays that are seen in Fig. 8 is the reverse MC to SP photoconversion under the action of the 532 nm probe light and not thermal reversion.

Before proceeding to the kinetic analysis, let's first take time out to experimentally validate the approach developed here in part 3 of the experimental section, the main conclusion of which, was that $\Delta R(r_{02})$ is a straight line with a slope proportional to k and the intercept proportional to Δn (eqn (9)–(11)). To validate this conclusion, a quasi-photostationary point was generated to achieve the maximum change in k and Δn for 2 different wavelengths of the probe laser one at 532 nm, where MC absorbs and we would expect to observe the effect of k, and the other at 671 nm, at which MC does not absorb, which means that $k = 0$ and only Δn contributes to the reflectance change.

This was achieved by irradiating the sample sequentially by the 355 nm pump pulses until ΔR was nearly saturated due to the combined photochemical reverse reactions caused by the pump (355 nm) and probe lasers (532 nm). This took about 15 shots of the pump laser using a repetition rate of ~0.75 pulse per second and a fluence of 10 mJ cm^{-2}. The 532 nm intensity used in this case was 2 mW cm^{-2}. After the reflectance change was nearly saturated, no more pump shots were applied, and R decayed by the action of the probe light until it reached its initial value. We repeated this process at different angles of incidence, keeping the 532 nm fluence the same. The r_{02} dependence of the reflectance near the saturation point, R_{sat}, when the 532 nm probe was used, is shown in Fig. 10a by a solid line. The dashed line shows the initial $R_{init}(r_{02})$. Fig. 10b shows the difference $\Delta R_{sat}(r_{02}) = R_{sat}(r_{02}) - R_{init}(r_{02})$. The corresponding dependences for the 671 nm probe are shown in Fig. 11a,b.

It can be seen, from Fig. 10 and 11, that for the 532 nm probe $R_{sat}(r_{02})$ is predominantly shifted horizontally with respect to $R_{init}(r_{02})$ after photoconversion, whilst in the case of the 671 nm probe the shift is mainly vertical. Consequently, $\Delta R_{sat}(r_{02})$ in Fig. 10b is a straight line with a significant slope in the case

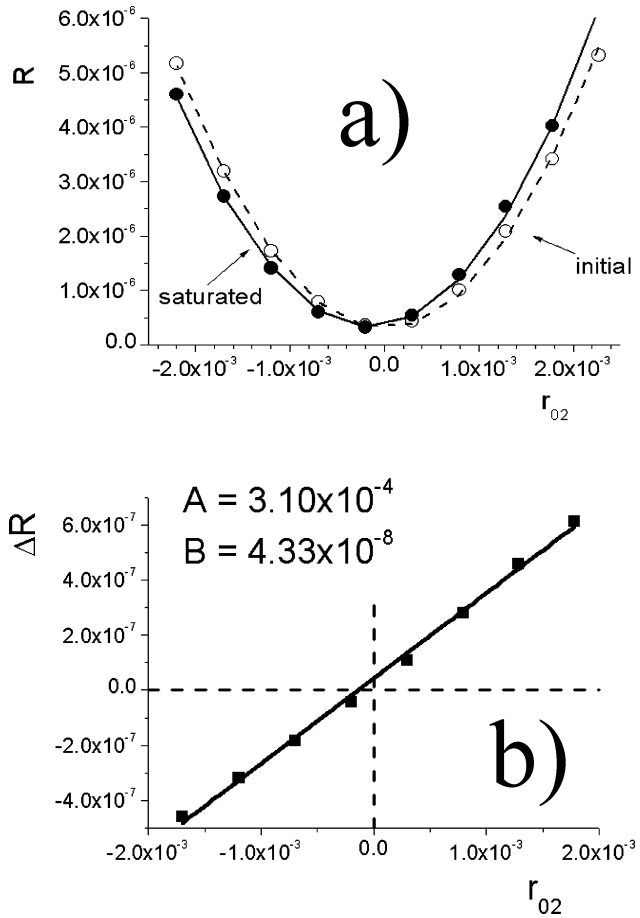

Fig. 10 r_{02} dependence of (a) saturated reflectance (solid line) and initial reflectance (dashed line) and (b) their difference using 532 nm probe light, 2 mW cm^{-2}. Reflectance was saturated by a train of 15 355 nm pulses of 10 mJ cm^{-2}, 0.75 pulse per second repetition rate.

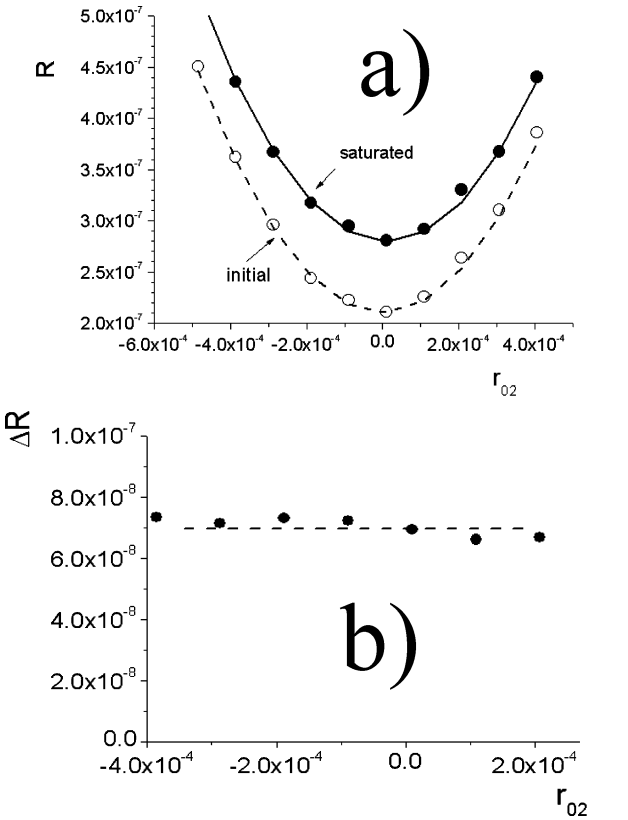

Fig. 11 r_{02} dependence of (a) saturated reflectance (solid line) and initial reflectance (dashed line) and (b) their difference using 671 nm probe light, 500 mW cm^{-2}. Reflectance was saturated by a train of 15 355 nm pulses of 10 mJ cm^{-2}, 0.75 pulse per second repetition rate.

of the 532 nm probe, whilst in the case of the 671 nm probe in Fig. 11b the slope is much smaller. Using formulae (9)–(12) and taking the parameters of the initial monolayers to be $d \approx 1.7$ nm and $n_{10} \approx 1.55$, as they were estimated above, the values of k and Δn were calculated. For the 532 nm probe $k \approx 2 \times 10^{-2}$ (Abs $\approx 5.6 \times 10^{-4}$) and $\Delta n \approx 2 \times 10^{-3}$. For the 671 nm probe $\Delta n \approx 4 \times 10^{-3}$. From the absorbance so-obtained from the 532 nm probe it is easy to estimate that the fraction of SP molecules photoconverted to MC $\Delta N_{MC} \approx 0.1$ nm^{-2}, which is only about 10% of the initial coverage close to saturation. For this estimate, ε for MC of 40 000 L mol^{-1} cm^{-1} at 532 nm and ε for SP of 4000 L mol^{-1} cm^{-1} at 355 nm was again assumed. Note, that for the 671 nm probe Δn is about twice as big as for the 532 nm probe as will be discussed next.

In the spectral regions where MC absorbs, dispersion of the real part of the refractive index can reach quite large values, as determined *via* the Kramers–Kronig relation.[35d] In the current case, the 532 nm probe light is close to the absorption maximum of MC, and according to the Kramers–Kronig relation, the refractive index dispersion is zero at absorption maxima. Therefore, we can assume that at both probe wavelengths the refractive index of the monolayer should be dispersion free and would change similarly upon SP to MC photoconversion.

As previously mentioned, the relationship between the real part of the refractive index and the relative surface concentration is not straightforward. In ellipsometry the Lorentz–Lorenz relation is commonly used.[35e] In this case, when the conversion is relatively small, it can be assumed that the refractive index change is proportional to the relative concentration of MC. Since with the 671 nm probe Δn is twice as high as at 532 nm, we can then conclude that the conversion of SP to MC in the case of the reflectance saturation at 671 nm is twice as high as the conversion in the case of the reflectance saturation at 532 nm. This is reasonable since there would be no photochemical reverse reaction due to the probe beam when probing with 671 nm light.

Next, we will discuss the kintetics of this system in detail. In Fig. 10b the slope of the ΔR_{sat} dependence is $A = 3.1 \times 10^{-4}$ and the intercept $B = 4.3 \times 10^{-8}$. Therefore, for $r_{02} \geq 10^{-3}$, the first term of eqn (9), Ar_{02}, will be significantly higher than the second term, B. For such values of r_{02}, B can be neglected in $\Delta R(r_{02})$, so that $\Delta R(r_{02}) \approx Ar_{02}$ and is proportional to the absorbance (from eqn (12)) and hence to the surface coverage of MC. Δn can then be safely ignored.

The reflectance change following a single excitation pulse is much smaller than the reflectance change at saturation (Fig. 10). Hence, the corresponding changes Δn and k will also be smaller. However the B coefficient can still be safely ignored for values of $r_{02} \geq 10^{-3}$. Therefore we can monitor $\Delta R(t)$ following a single 355 nm pulse at a fixed angle of incidence corresponding to one such r_{02} value and we can still expect that $\Delta R(t)$ will be proportional to the MC surface concentration. We can then obtain kinetic information directly from $\Delta R(t)$.

 This journal is © The Royal Society of Chemistry and Owner Societies 2010

A representative dependence $\Delta R(t)$ at $r_{02} = 10^{-3}$, following a single 355 nm excitation pulse (10 mJ cm^{-2}) is shown in Fig. 12. For this trace a 532 nm probe intensity of 36 mW cm^{-2} was used. The decay adequately fits to a biexponential function with exponents having decay times differing by 5 times (τ_1, τ_2) and having similar amplitudes. It is known that steric and site-dependent matrix effects can play a crucial part in SP/spirooxazine photoisomerizations.[39,40] Therefore, we can assign the difference in the decay times to inhomogeneity of the molecular environment within the monolayer. Since the amplitudes of the exponents are similar, the amounts of molecules in different environments are probably almost equal. Of course the real situation is likely to be more complex than biexponential, however the approximation fits in this case.

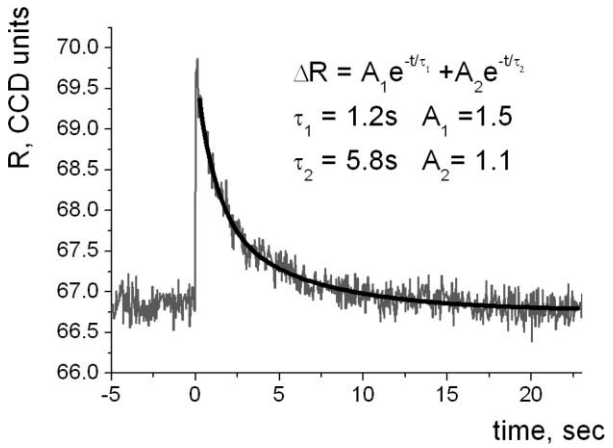

Fig. 12 Representative dependence $\Delta R(t)$ at $r_{02} = 10^{-3}$ following a single 355 nm pulse (10 mJ cm^{-2}) and its biexponential approximation. 532 nm probe, 36 mW cm^{-2}.

Fig. 13 shows the dependence of the fast (open circles) and the slow (closed triangles) components' reciprocal lifetimes on the 532 nm light intensity. Both dependences were fitted linearly. In both cases the intercept is zero at zero laser intensity, which confirms that the $\Delta R(t)$ decay occurs solely due to the action of the 532 nm probe light. From the slopes of the reciprocal lifetime dependences we can estimate quantum efficiencies for both components in the biexponential decay: $\tau^{-1} = \sigma q \Phi_{532}$, where σ is the absorption cross section in cm^2, q is the quantum efficiency of MC to SP photoconversion, Φ_{532} is the photon flux of the 532 nm light in cm^{-2} s^{-1}. The corresponding quantum efficiencies were estimated to be $q_1 \approx 0.2$ for the fast component and $q_2 \approx 0.03$ for the slow component, which are reasonable values based on data obtained in a solid matrix.[36]

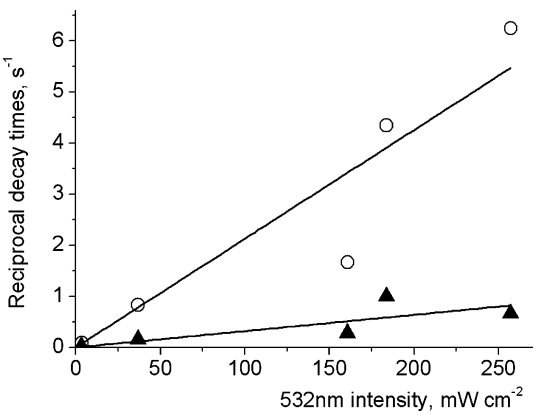

Fig. 13 Reciprocal lifetimes of the R decay biexponential approximation *vs.* 532 nm probe light intensity. Open circles: fast component; closed triangles: slow component of the approximation. Solid lines: linear fittings of the experimental data.

Fig. 14 shows the typical 355 nm excitation pulse fluence dependence of ΔR taken at the moment just after the 355 nm excitation pulse, $t = 0$. The angle of incidence was fixed so that $r_{02} = 2 \times 10^{-3}$. The left y-axis corresponds to ΔR. Since in our case ΔR is simply proportional to the monolayer absorbance, ΔR can be recalculated into absorbance using eqn (9) and (12). These calculated absorbance values correspond to the right y-axis. One can see that the dependence is saturated at excitation fluences higher than 30 mJ cm^{-2}. The level of the absorbance saturation is about 3×10^{-4}. This saturation is achieved using single pulse laser excitation with relatively high pulse fluence at the point of saturation. This is in contrast to the saturation achieved by a sequence of low-fluence pulses that was used to obtain the data in Fig. 10 and 11. In fact, the level of the saturated absorbance for single pulse excitation is about half that for the multi-pulse saturated absorbance.

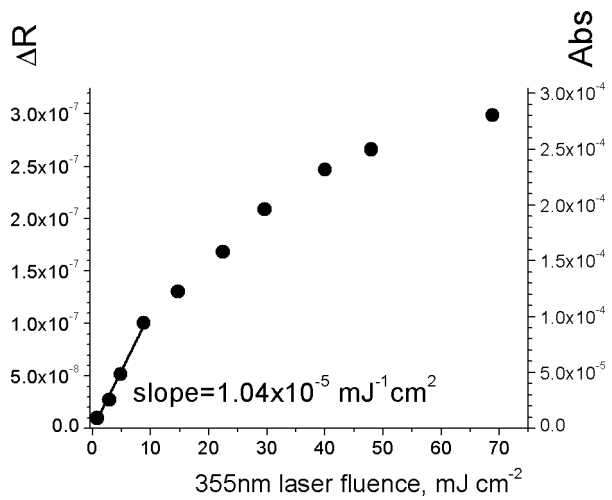

Fig. 14 355 nm fluence dependence of the initial reflectance change measured just after a 355 nm pulse. Reflectance change is shown on the left y-axis. The corresponding absorbance is shown on the left y-axis. 532 nm probe light, 2 mW cm^{-2}; $r_{02} = 2 \times 10^{-3}$.

This is no doubt due to the absorption cross section becoming saturated in case of single pulse saturation, since the condition $\sigma\Phi \ll 1$ is not satisfied for fluences higher than 30 mJ cm^{-2} ($\sigma\Phi \approx 0.5$ for 50 mJ cm^{-2}).

For low fluences <10 mJ cm^{-2}, the dependence is approximated to be linear. From the slope of the dependence we can estimate the average quantum efficiency of the SP $\rightarrow$ MC conversion under action of the 355 nm light. It was found to be $q_{sp}^{355} \approx 0.1$, which is again a reasonable value for this type of transformation in a solid matrix.[36,40] Fig. 15 shows two kinetic traces of $\Delta R(t)$ corresponding to two extreme points in Fig. 14. Fig. 15a corresponds to the point with the highest 355 nm fluence used (about 70 m Jcm^{-2}). Fig. 15b corresponds to the point with the lowest 355 nm fluence

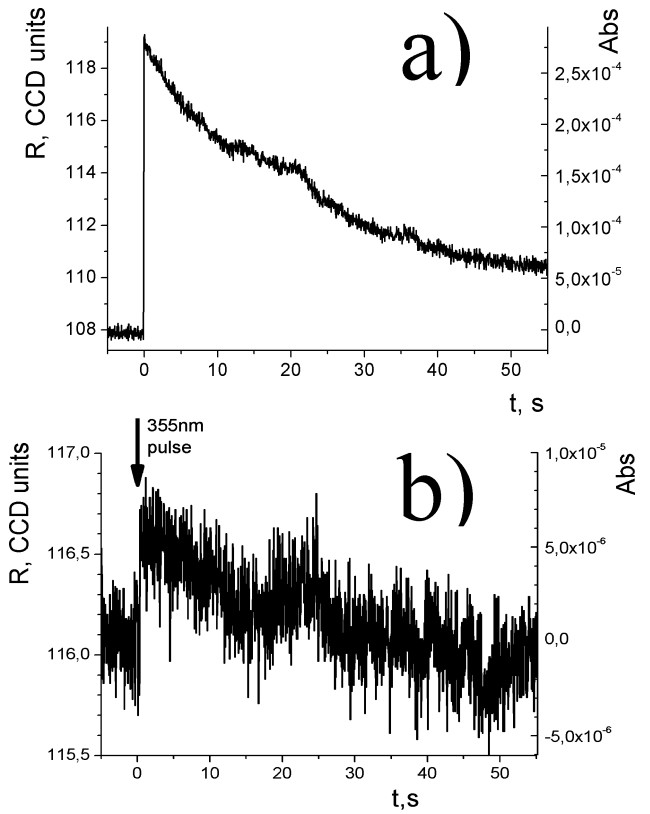

Fig. 15 $\Delta R(t)$ corresponding to two points in Fig. 12: (a) the point with the highest 355 nm fluence used (about 70 mJ cm^{-2}); (b) the point with the lowest 355 nm fluence used (about 1 mJ cm^{-2}).

used (about 1 mJ cm^{-2}). The maximum ΔR at $t = 0$ in Fig. 15a corresponds to an absorbance of 2.8×10^{-4} and that in Fig. 15b corresponds to an absorbance of about 6×10^{-6}. From this figure we can estimate the single-shot detection limit of our method with respect to absorbance as ~10^{-6}. Note that this detection limit may improve as more stable laser sources and higher dynamic range detectors may be used. The kinks in the curves are due to long term probe laser stability drift. The higher frequency noise comes from the laser and the CCD. If kinetics were not require then a lock in amplifier could also improve the detection limit. Referencing the laser beam or using a more stable source can probably improve the sensitivity as could using a cooled CCD. In any case, in its current form, the method is at least comparable to the best alternative methods currently available.[17,22–30,32]

D. Conclusions

SP and MC photochemistry on an immobilized quartz monolayer was studied using time-resolved Brewster angle reflectometry. The quantum efficiency for SP to MC conversion was 0.1, whereas the conversion from MC to SP occurred with yields of 0.2 and 0.03. The thermal reverse reaction was negligible over 10 min. This new method in photochemistry can give information on both real and imaginary refractive index changes for transient species. The single shot transient detection limit is currently sensitive to absorbance changes of ~10^{-6}.

Acknowledgements

This work has been mainly funded by in-house IMRE core funding and partially supported by Joint Council Office funding from A*STAR, Singapore.

References

1 S. Wang, Y. Song and L. Jiang, Photoresponsive surfaces with controllable wettability, *J. Photochem. Photobiol., C*, 2007, **8**, 18.
2 R. Rosario, D. Gust, M. Hayes, F. Jahnke, J. Springer and A. A. Garcia, Photon-modulated wettability changes on spiropyran-coated surfaces, *Langmuir*, 2002, **18**, 8062.
3 A. Athanassiou, M. Varda, E. Mele, M. I. Lygeraka, D. Pisignano, M. Farsari, C. Fotakis, R. Cingolani and S. H. Anastasiadis, Combination of microstructuring and laser irradiation for the reversible wettabiltiy of photosensitised polymer surfaces, *Appl. Phys. A: Mater. Sci. Process.*, 2006, **83**, 351.
4 H. Tachibana, Y. Yamanaka, H. Sakai, M. Abe and M. Matsumoto, J-aggregate formation of amphiphilic merocyanine in Langmuir-Blodgett films, *J. Lumin.*, 2000, **87–89**, 800.
5 M. Matsumoto, Photoreactions and lateral patterning in Langmuir and Langmuir-Blodgett films, *Chem. Rec.*, 2007, **7**, 69.
6 K. Balashev, I. Panaitov and J. E. Proust, Propagation of photoinduced surface pressure perturbation along a mixed benzospiropyran-octadecanol monolayer, *Langmuir*, 1997, **13**, 5373.
7 J. Hobley, T. Oori, S. Gorelik, S. Kajimoto, H. Fukumura and D. Hönig, Time-resolved Brewster angle microscopy for photochemical and photothermal studies on thin-films and monolayers, *J. Nanosci. Nanotechnol.*, 2008, **8**, 1.
8 J. Hobley, T. Oori, S. Kajimoto, S. Gorelik, K. Hatanaka, D. Hönig and H. Fukumura, Laser-induced phase change in Langmuir films observed using nanosecond pump–probe Brewster angl microscopy, *Appl. Phys. A: Mater. Sci. Process.*, 2008, **93**, 947.
9 M. J. Lear and J. Hobley, You make it, I break it, *COSMOS*, 2008, **4**, 99.
10 E. Katz, B. Willner and I. Willner, Light-controlled electron transfer reactions at photoisomeririzable monolayer electrodes by means of electrostatic interactions: active interfaces for amperometric transduction of recorded optical signals, *Biosens. Bioelectron.*, 1997, **12**(8), 703.
11 B. Mecheri, P. Baglioni, O. Pieroni and G. Caminati, Molecular switching in nano-structured photochromic films of biopolymers, *Mater. Sci. Eng., C*, 2003, **23**, 893.
12 E. Aznar, R. Casasus, B. Garcia-Acosta, M. D. Marcos, R. Martinez-Manez, F. Sancenon, J. Soto and P. Amoros, Photochemical and chemical two-channel control of functional hybrid architectures, *Adv. Mater.*, 2007, **19**, 2228.
13 T. Seki, Dynamic photoresponsive functions in organized layer systems comprised of azobenzene-containing polymers, *Polym. J.*, 2004, **36**(6), 435.
14 Y.-G. Mo, R. O. Dillon, P. G. Snyder and T. E. Tiwald, Optical properties of photochromic organic-inorganic composites, *Thin Solid Films*, 1999, **355**, 1.
15 Y.-G. Mo, R. O. Dillon and P. G. Snyder, Spectroscopic analysis of photochromic films, *J. Vac. Sci. Technol., A*, 1999, **17**(1), 170.
16 S.-H. Kim, H.-J. Suh, K.-N. Koh, S.-A. Suck, H.-J. Choi and H.-S. Kim, Surface plasmon resonance study on the interaction between photochromic spironaphthoxazine with L-phenylalanine in self assembled monolayers on gold, *Dyes Pigm.*, 2004, **62**, 93.
17 K. Sasaki and T. Nagamura, Ultrafast all-optical switch using complex refractive index changes of thin films containing photochromic dyes, *Appl. Phys. Lett.*, 1997, **71**(4), 434.
18 P. Kubelka and F. Munk, Ein Beitrag zur optik der farbanstriche, *Z. Tech. Phys.*, 1931, **12**, 593.
19 F. Wilkinson and C. J. Willsher, The use of diffuse reflectance laser flash photolysis to study primary photoprocesses in anisotropic media, *Tetrahedron*, 1987, **43**(7), 1197.
20 G. P. Kelly, P. A. Leicester, F. Wilkinson, D. R. Worrall, L. F. Vieira Ferreira, R. Chittock and W. toner, Picosecond diffuse reflectance and transmission laser photolysis study of various triaryl-2-pyrazolines, *Spectrochim. Acta, Part A*, 1990, **46**(6), 975.
21 M. Ichikawa, H. Fukumura and H. Masuhara, Picosecond regular reflection spectroscopic study on ultrafast heat generation in copper phthalocyanine solid, *J. Phys. Chem.*, 1994, **98**, 12211.

 This journal is © The Royal Society of Chemistry and Owner Societies 2010

22 H. Kawai, K. Nakano and T. Nagamura, White light optical waveguide detection of transient absorption spectra in ultrathin organic films upon pulsed laser excitation, *Chem. Lett.*, 2001, 1300.
23 D. Kleine, J. Lauterbach, K. Kleinermans and P. Hering, Cavity ring-down spectroscopy of molecularly thin iodine films, *Appl. Phys. B: Lasers Optics*, 2001, **72**, 249.
24 J. A. Piest, M. Anni, R. Cingolani and G. Gigli, Singlet to triplet excitation spectrum of thin film tris-(8-hydroxyquinolate)-aluminium in direct absorption, *Synth. Met.*, 2008, **158**, 1062.
25 I. M. P. Aarts, B. Hoex, A. H. M. Smets, R. Engeln, W. M. M. Kessels and M. C. M. van de Sanden, Direct and highly sensitive measurement of defect-related absorption in amorphous silicon thin films by cavity ring-down spectroscopy, *Appl. Phys. Lett.*, 2004, **84**(16), 3079.
26 R. N. Muir and A. J. Alexander, Structure of monolayer dye films studied by Brewster angle cavity ring-down spectroscopy, *Phys. Chem. Chem. Phys.*, 2003, **5**, 1279.
27 C. Zhu, B. Xiang, L. Zhu and R. Cole, Determination of absorption cross sections of surface adsorbed HNO_3 in the 290–330nm region by Brewster angle cavity ring-down spectroscopy, *Chem. Phys. Lett.*, 2008, **458**, 373.
28 X. Wang, M. Hinz, M. Vogelsang, T. Welsch, D. Kaufmann and H. Jones, A new approach to detecting biologically active substances with evanescent wave cavity ring-down spectroscopy, *Chem. Phys. Lett.*, 2008, **467**, 9.
29 R. Katoh, A. Furube, A. V. Barzykin, H. Arakawa and M. Tachya, Kinetics and mechanism of electron injection and charge recombination in dye-sensitized nanocrystalline semiconductors, *Coord. Chem. Rev.*, 2004, **248**, 1195.
30 T. Yoshihara, M. Murai, Y. Tamaki, A. Furube and R. Katoh, Trace analysis by transient absorption spectroscopy: estimation of the solubility of C_{60} in polar solvents, *Chem. Phys. Lett.*, 2004, **394**, 161.
31 R. Teppner, S. Bae, K. Haage and H. Motschmann, On the Analysis of Ellipsometric Measurements of Adsorption Layers at Fluid Interfaces, *Langmuir*, 1999, **15**, 7002–7009.
32 B. L. Frey, R. M. Corn and S. C. Weibel, Polarization-Modulation Approaches to Reflection-Absorption Spectroscopy, in *Handbook of Vibrational Spectroscopy*, ed. J. Chalmers and P. R. Griffiths, John Wiley & Sons, Chichester, UK, 2001, vol. 2. pp. 1042–1056.
33 S. Henon and J. Meunier, Microscope at the Brewster-angle – Direct observation of 1st-order phase transitions in monolayers, *Rev. Sci. Instrum.*, 1991, **62**(4), 936.
34 D. Hönig and D. Möbius, Direct visualisation of monolayers at the air–water interface by Brewster-angle microscopy, *J. Phys. Chem.*, 1991, **95**(12), 4590.
35 (*a*) H. Fujiwara, *Spectroscopic Ellipsometry, Principles and applications*, Wiley, West Sussex, England, 2007, p. 33; (*b*) p. 46; (*c*) p. 26; (*d*) p. 176; (*e*) p. 178.
36 D. A. Reeves and F. Wilkinson, Photochromism of Spiropyrans: Part 1. Mechanism of photocolouration, *J. Chem. Soc., Faraday Trans. 2*, 1973, **69**, 1381.
37 *CRC Handbook, Refractive index and transmittance of representative glasses*, CRC Press, Boca Raton, Florida, 79th edn, 1998–1999, pp. 10–217.
38 J. Hobley, V. Malatesta, R. Millini, L. Montanari and W. O. N. Parker Jr, Proton exchange and isomerization reactions of photochromic and reverse photochromic spiro-pyrans and their merocyanine forms, *Phys. Chem. Chem. Phys.*, 1999, **1**, 3259.
39 J. M. Galvin and G. B. Schuster, Preparation and characterization of mixed thin films containing spiropyrans and long chain alkyl silanes: towards a command of surfaces for liquid crystal realignment, *Supramol. Sci.*, 1998, **5**, 89.
40 J. Hobley and F. Wilkinson, Photochromism of naphthoxazine-spiro-indolines by direct excitation and following sensitisation by triplet-energy donors, *J. Chem. Soc., Faraday Trans.*, 1996, **92**(8), 1323.